LETTERS

Glacier retreat in New Zealand during the Younger Dryas stadial

Michael R. Kaplan[1], Joerg M. Schaefer[1,2], George H. Denton[3], David J. A. Barrell[4], Trevor J. H. Chinn[5], Aaron E. Putnam[3], Bjørn G. Andersen[6], Robert C. Finkel[7,8], Roseanne Schwartz[1] & Alice M. Doughty[9]

Millennial-scale cold reversals in the high latitudes of both hemispheres interrupted the last transition from full glacial to interglacial climate conditions. The presence of the Younger Dryas stadial (~12.9 to ~11.7 kyr ago) is established throughout much of the Northern Hemisphere, but the global timing, nature and extent of the event are not well established. Evidence in mid to low latitudes of the Southern Hemisphere, in particular, has remained perplexing[1–6]. The debate has in part focused on the behaviour of mountain glaciers in New Zealand, where previous research has found equivocal evidence for the precise timing of increased or reduced ice extent[1–3]. The interhemispheric behaviour of the climate system during the Younger Dryas thus remains an open question, fundamentally limiting our ability to formulate realistic models of global climate dynamics for this time period. Here we show that New Zealand's glaciers retreated after ~13 kyr BP, at the onset of the Younger Dryas, and in general over the subsequent ~1.5-kyr period. Our evidence is based on detailed landform mapping, a high-precision ^{10}Be chronology[7] and reconstruction of former ice extents and snow lines from well-preserved cirque moraines. Our late-glacial glacier chronology matches climatic trends in Antarctica, Southern Ocean behaviour and variations in atmospheric CO_2. The evidence points to a distinct warming of the southern mid-latitude atmosphere during the Younger Dryas and a close coupling between New Zealand's cryosphere and southern high-latitude climate. These findings support the hypothesis that extensive winter sea ice and curtailed meridional ocean overturning in the North Atlantic led to a strong interhemispheric thermal gradient[8] during late-glacial times, in turn leading to increased upwelling and CO_2 release from the Southern Ocean[9], thereby triggering Southern Hemisphere warming during the northern Younger Dryas.

The transition of Earth's climate from the last ice age to the warm conditions of the Holocene epoch (the past ~11.5 kyr) is not yet fully explained. Polar ice-core records show that during this transition a period of general warming was interrupted in each hemisphere. The Antarctic cold reversal (ACR), as defined by a distinct levelling off or slight reversal of warming over Antarctica between ~14.5 and ~12.9 kyr ago, is mirrored by parallel deglacial changes in atmospheric CO_2 (ref. 10). Subsequently, Antarctic temperatures and atmospheric CO_2 concentrations increased and reached full interglacial values by ~11.5 kyr ago. In the North Atlantic region, the Younger Dryas stadial (YDS) period between ~12.9 and ~11.7 kyr ago[11,12] saw annual temperatures cool by ~15 °C in Greenland (and perhaps farther afield from there) despite steadily increasing global atmospheric CO_2 concentrations[13,14]. The YDS coincided with weakened intensity of the Asian monsoon[15], cooler sea surface temperatures in the tropical Atlantic[16] and increased precipitation in Brazil as far south as 28 °S[17].

Thus, the sea surface temperature signature of the YDS can be traced south to at least the northern tropics, and affected precipitation patterns even in the southernmost tropics[17]. Outstanding questions include determining the location of the southern boundary of the YDS climate imprint, the nature of the transition to the 'ACR-type' climate that is recorded in southern polar latitudes and the place where this transition occurred. We investigate past atmospheric conditions in the southern mid latitudes to find a missing piece of the jigsaw puzzle of late-glacial climate. New Zealand's oceanic island setting in the southwest Pacific Ocean is ideal for testing hypotheses concerning late-glacial climate change, far from the influence of Northern Hemisphere ice sheets and the North Atlantic deep-water convection. So far, studies in the New Zealand region have shown ambiguous signatures of late-glacial climate. Some records show a late-glacial reversal spanning both the ACR and the YDS time interval, and others display dominant imprints of the ACR (see, for example refs 1–4, 18–20).

We report here on a cirque basin, of about 7-km^2 extent, at the head of Irishman Stream in the Ben Ohau range on the eastern side of the Southern Alps of South Island, New Zealand (Fig. 1). This basin was purposely chosen for study because of its outstanding suitability for quantifying palaeoclimate (Supplementary Information). The moraines of the Irishman basin are exceptionally well preserved and the topographic setting allows the former glaciers to be reconstructed to a high degree of certainty. As a result, precise limits can be placed on the dimensions and snow lines associated with these glaciers. Furthermore, the basin floor gradients are such that the former glacier was particularly sensitive to small climate fluctuations. To track late-glacial glacier dynamics in detail, we produced a geomorphic map (~1:10,000 scale), which forms the foundation for a comprehensive, precise and accurate ^{10}Be chronology[7] based on a nearby production rate calibration of high precision[21]. To evaluate the amplitude of late-glacial climate changes, we reconstructed the former glacier extents and estimated their commensurate equilibrium line altitudes (ELAs).

South Island glaciers are very responsive to climate fluctuations, particularly variations in summer temperatures. Consequently, response times for glaciers of the sizes that existed in Irishman basin are on the order of years[22,23]. The glacier in the Irishman basin recorded atmospheric changes well above sea level, between ~1,700 and ~2,300 m. Our chronology of glacier and snow-line changes is thus interpreted to represent a centennial-scale proxy record of regional

[1]Lamont-Doherty Earth Observatory, Geochemistry, Palisades, New York 10964, USA. [2]Department of Earth and Environmental Sciences, Columbia University, New York, New York 10027, USA. [3]Department of Earth Sciences and Climate Change Institute, University of Maine, Orono, Maine 04469, USA. [4]GNS Science, Private Bag 1930, Dunedin 9054, New Zealand. [5]Alpine and Polar Processes Consultancy, Lake Hawea, Otago 9382, New Zealand. [6]Department of Geosciences, University of Oslo, 0316-Oslo, Norway. [7]Department of Earth and Planetary Sciences, University of California, Berkeley, California 95064, USA. [8]CEREGE, 13545 Aix-en-Provence, Cedex 4, France. [9]Antarctic Research Centre and School of Earth Sciences, Victoria University of Wellington, PO Box 600, Wellington 6140, New Zealand.

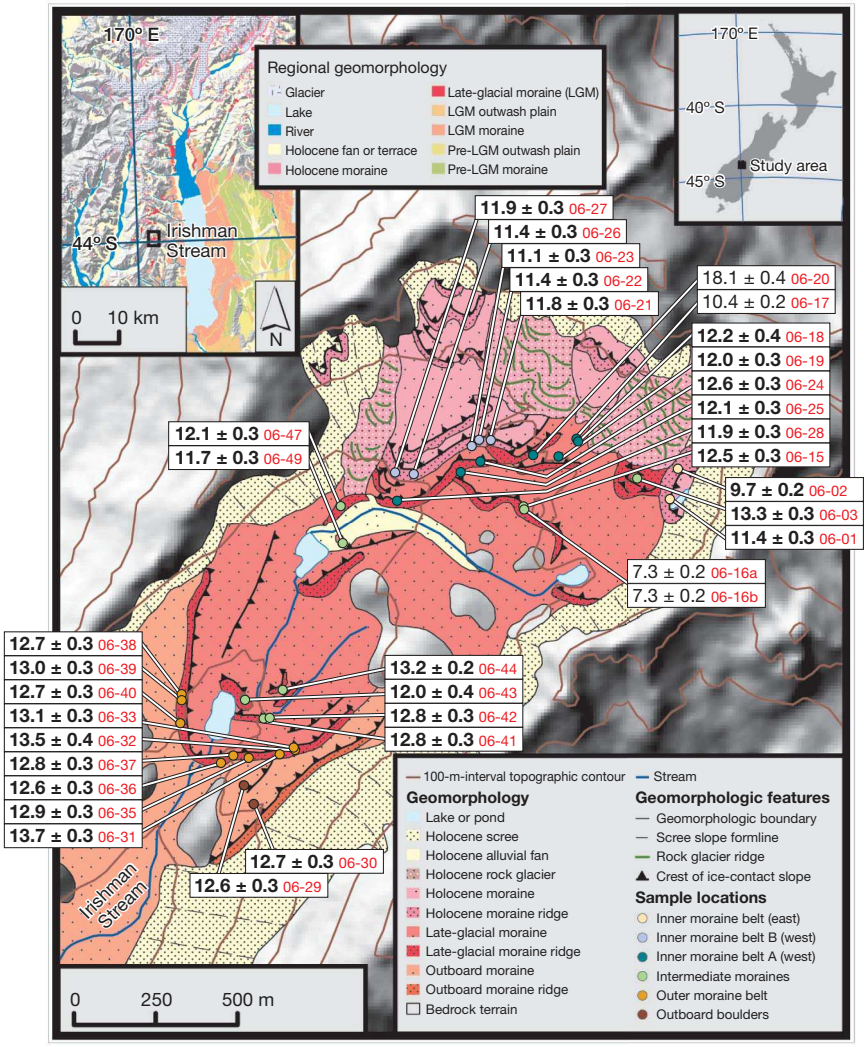

Figure 1 | Glacial geomorphology map of the moraines in the Irishman basin, showing locations of sample sites and measured ^{10}Be ages. The map (~1:10,000 scale) differentiates between discrete moraine ridges and areas of more diffuse moraine[28]. Individual ages are shown in kiloyears with their 1σ analytical errors. Outliers are in non-bold. Systematic uncertainties, such as that associated with the production rate, are minimal when comparing ages of adjacent moraines. Inset maps show location on South Island (top right) and in relation to adjacent major valley systems (top left).

atmospheric conditions, especially summer conditions, for South Island.

Well-defined moraine ridges are preserved in the outer and inner parts of the Irishman basin. Most striking is a prominent, very well-preserved, arcuate moraine that was a focus of our study (Fig. 1). We refer to this moraine as 'the outer moraine belt'. On its down-valley (outboard) side lies very subdued morainal and ice-smoothed bedrock topography, with few distinct moraine features (Supplementary Information). The inner parts of the basin, within ~0.75 km of the headwall, contain a set of two prominent ridges, referred to here as 'inner moraine belt A' and 'inner moraine belt B'. Between the outer moraine belt and inner moraine belts A and B, there are a few discontinuous 'intermediate' moraine ridges. Up-valley of inner moraine belt B, within 100 to 200 m of the headwall, are several small moraine ridges partly overlain by subsequent scree and rock-glacier (that is, mass-creep) deposits.

We sampled large boulders protruding from the moraine deposits in the Irishman basin. Analytical results and ages are presented in Fig. 1 and in Supplementary Tables 1 and 2. Individual ^{10}Be data are shown with 1σ analytical uncertainties, and the arithmetic mean ages of moraines are presented with an error that includes propagation of the analytical uncertainty and the uncertainty in the local production rate (Supplementary Fig. 4). The data set is of high internal consistency and only three out of 37 ages are considered outliers (IS-06-16, IS-06-17 and IS-06-20; Fig. 1). All nine ^{10}Be ages from the outer moraine belt are normally distributed and have a high internal consistency ($\chi^2 = 1.3$). They range from 13.7 ± 0.3 to 12.6 ± 0.3 kyr, with a mean of 13.0 ± 0.5 kyr. Four samples from the outermost of the intermediate ridges yielded a statistically indistinguishable mean age of 12.7 ± 0.6 kyr. Farther inboard, three ^{10}Be ages from inner intermediate ridges yield a mean age of 12.1 ± 0.5 kyr. On inner moraine belt A (Fig. 1), five boulders yield a mean age of 12.2 ± 0.4 kyr, which is statistically indistinguishable from that determined from the inner intermediate ridges. On inner moraine belt B, five boulders range in age from 11.9 ± 0.3 to 11.1 ± 0.3 kyr, with a mean age of 11.5 ± 0.4 kyr ($\chi^2 = 1.4$). Collectively, the moraine ages in the Irishman basin are sufficiently precise to bracket an overall period of reduction in glacier size over ~1.5 kyr, from ~13.0 to ~11.5 kyr ago.

The ^{10}Be chronology indicates that most of the moraine sequence in the Irishman basin was formed during late-glacial time. The prominent ~13-kyr moraine represents a distinct glacier terminal position,

probably in equilibrium with the climate prevailing at the time. Between ~13 and ~12 kyr ago, the record attests to a large change in glacier dimensions and overall recession, with no prominent moraines deposited during this time. By ~12 kyr ago, the glacier was much less than half of its 13-kyr ice extent (Figs 1 and 2). By ~500 yr later, the glacier had built another moraine less than 100 m farther inboard (Fig. 1). This moraine indicates the glacier position at the Pleistocene/Holocene boundary, the end of the YDS. The ~12- and ~11.5-kyr inner moraine belts A and B represent the most important pauses in general retreat up the basin after ~13 kyr ago, and were built by a glacier of much smaller dimensions. We cannot determine whether recession and re-advance preceded the formation of inner moraine belts A and B, or whether these moraines simply represent stillstands during recession.

We reconstructed the geometries of the former glacier when the margin was at the outer moraine belt and inner moraine belt A terminal positions. From these reconstructions, we estimated the formative ELAs and associated climate changes (Supplementary Information). Between ~13 and ~12 kyr ago, the ELA rose by 75 ± 40 m. Assuming an adiabatic lapse rate of 0.6–1° per 100 m, this ELA change translates into a warming of between ~0.25 and ~1 °C (neglecting precipitation change). The ELA at ~11.5 kyr ago was slightly higher than at ~12 kyr ago, but the difference was probably of the order of metres, judging by the <100-m separation between inner moraine belts A and B.

The Irishman basin results represent a sampling of late-glacial atmospheric conditions over New Zealand. This precisely dated record of late-glacial moraines, where former snow lines are also precisely quantified as proxies for atmospheric conditions, is unique. We look to other record types for comparison and confirmation of the regional significance of the findings. Vegetation and chironomid data from the intermontane valleys and basins of the Southern Alps show that climatic amelioration, with some variability, occurred between ~13 and ~11.5 kyr ago[1,18–20]. At Kaipo bog on northeastern North Island, very well-dated vegetation changes[1,19] (Fig. 2) indicate a return to cooler conditions shortly before, and warming near the onset of and generally throughout, the YDS interval. Offshore to the east of North Island, the MD97-2121 core is linked directly to the Kaipo bog record by rhyolitic tephras common to both sites. These allow direct alignment of these palaeoclimate records independently of individual dating uncertainties[1]. At MD97-2121, isotopic and chemical properties of both benthic and planktonic fossils are used to infer a major pause in deglacial warming, beginning well before 13 kyr ago[24]. During the YDS interval, the late-glacial reversal ended with marked changes in bottom-water properties and general surface warmth, with variability, through to the Holocene[24].

Thus, high-resolution records from the southwest Pacific region and elsewhere, including Antarctica[1,6,25], show a consistent Southern Hemisphere late-glacial climatic signature of overall decreased ice extent or progressive warming, with fluctuations, between ~13 and ~11.5 kyr ago. Atmospheric CO_2 change and Southern Ocean dynamics exhibit a similar pattern (Fig. 2). Specifically, atmospheric CO_2 concentrations increased markedly, with some minor fluctuations between ~13 and ~11.5 kyr ago, linked closely with Southern Ocean upwelling intensity, during the YDS[9].

This study highlights an emerging capability to use precise and accurate ^{10}Be dating of well-mapped moraines to distinguish, with submillennial-scale resolution, between northern and southern climatic signatures[7]. The ~13-kyr outer moraine belt formed late in the ACR, as defined in Antarctica (Fig. 2). Throughout YDS time, the Irishman glacier became unequivocally smaller in comparison with its ~13-kyr size, and by ~12 kyr ago the ice had lost more than half its area and was almost at its 11.5-kyr limit. During this period of retreating glacier ice, rising snow lines and, thus, warmer temperatures, the

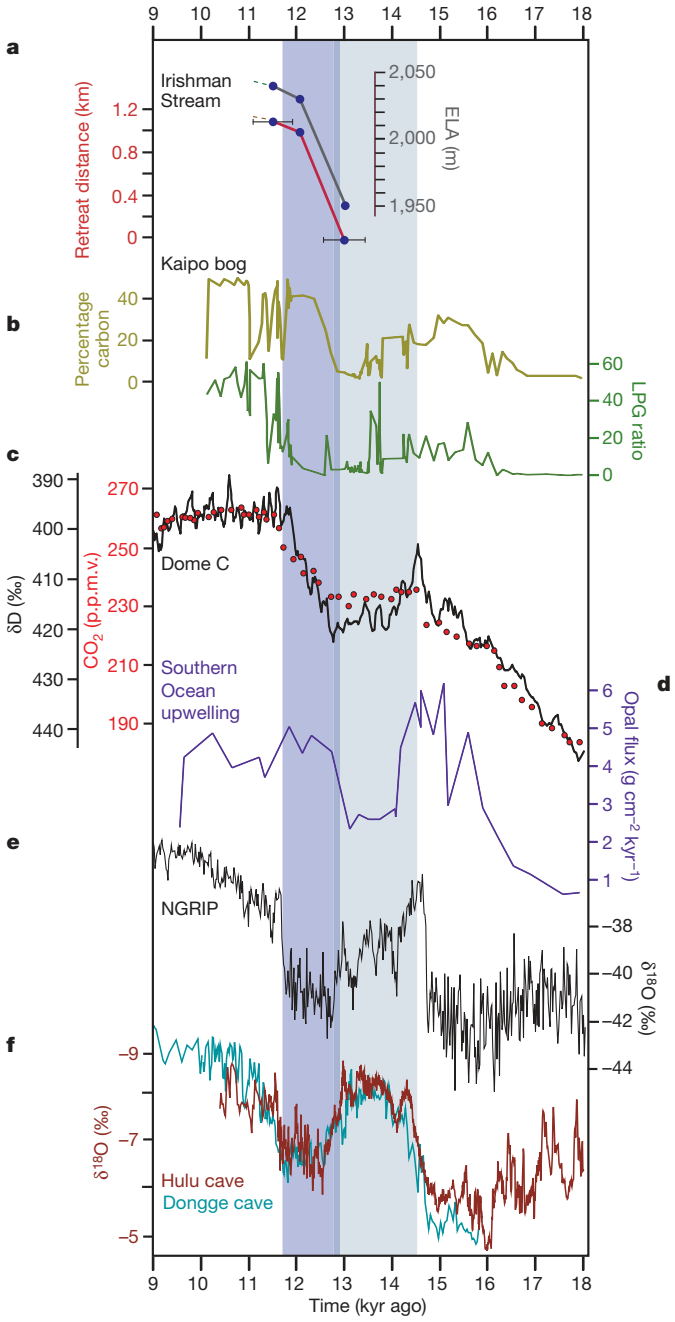

Figure 2 | Glacier changes in Irishman basin, New Zealand, in comparison with other climate proxy records. **a**, For the Irishman basin, glacier terminus retreat distance and ELA changes are shown for ~13.0 kyr, ~12 kyr and ~11.5 kyr BP, calculated on the basis of ^{10}Be dating of the moraines (Supplementary Information). Retreat distance is used to show the response of the glacier. We emphasize the pattern of change during the ~1.5-kyr interval for these two parameters. Age uncertainties for the ~13- and ~11.5-kyr moraines include the systematic uncertainties for production rate used, for comparison with other records. **b**, Carbon abundance (percentage carbon) and ratio of lowland podocarp to grass pollen (LPG) from Kaipo bog, North Island[19]. These proxies indicate the end of the late-glacial reversal and warming early on and through the YDS interval. The age model is based on midpoints of calibrated age ranges[19]. **c**, δD (deuterium) and CO_2 from European Project for Ice Coring in Antarctica (EPICA) Dome C[29,30]. The late-glacial ACR interrupted the prominent glacial-to-interglacial CO_2 increase. **d**, Opal flux from sediment core TN057-13PC[9]. Spanning the onset of the YDS, between ~13 and ~12 kyr ago, records **a**–**d** show warming in the Southern Hemisphere that matches closely the rise of CO_2 concentrations and variations in oceanic upwelling as recorded in the flux of opal. **e**, **f**, $\delta^{18}O$ $((^{18}O/^{16}O)_{sample}/(^{18}O/^{16}O)_{standard} - 1 \times 1{,}000$, where the standard is standard mean ocean water) from the North Greenland Ice Core Project[11] (NGRIP; **e**) and from the Hulu and Dongge caves, China[15] (**f**). Dark- and light-blue shaded regions represent the YDS and ACR cold periods, respectively[10,11,30].

only well-defined moraines are well inboard of the ~13-kyr moraine. Inner moraine belts A and B may represent brief fluctuations of climate, conceivably manifestations of variations seen in other Southern Hemisphere records (Fig. 2b, c), during the late YDS time interval, as defined in the Greenland ice core[11].

The results presented here support the hypothesis of a steep inter-hemispheric thermal gradient during the YDS[8]. Whereas North Atlantic mean annual temperatures dropped drastically, by at least 15 °C (refs 13, 14), atmospheric temperatures in the southern mid latitudes increased during this period (Fig. 2). A classic explanation for these observations is the bipolar seesaw mechanism[26,27], which proposes curtailment of North Atlantic overturning, leading to heat being retained in the Southern Hemisphere, increased formation of southern deep water and a warming of the Southern Ocean and the southern atmosphere. A recently proposed, complementary mechanism involves North Atlantic cold conditions paired with southward movement of northern sea ice cover leading to more extreme seasonality[14]. This would shift the intertropical convergence zone and westerly wind patterns[8,27] southwards, which has been shown to increase Southern Ocean upwelling and outgassing of CO_2 abruptly[9]. In this picture, during late-glacial times southern mid latitudes warm owing to CO_2 forcing and New Zealand glaciers should have exhibited marked retreat between ~13 and ~11.5 kyr ago, with the possibility of pauses mirroring minor fluctuations in the CO_2 increase (Fig. 2). It remains an open question as to how much of the warming was due to rising CO_2 concentrations and how much was due to hemispheric heat redistribution by means of the bipolar seesaw mechanism. Nonetheless, the striking match between our late-glacial observations and the atmospheric CO_2 concentration indicates a link among the behaviours of the Southern Ocean, the southern atmosphere, atmospheric CO_2 and New Zealand's temperatures as indicated in the activity of its cryosphere. To conclude, CO_2 increase and atmospheric warming seem to have been key influences on glacier behaviour in the southern mid latitudes during the transition from the last ice age to the present interglacial.

Received 20 February; accepted 22 June 2010.

1. Alloway, B. V. *et al.* Towards a climate event stratigraphy for New Zealand over the past 30,000 years (NZ-INTIMATE Project). *J. Quat. Sci.* **22,** 9–35 (2007).
2. Denton, G. H. & Hendy, C. H. Younger Dryas age advance of Franz Josef Glacier in the Southern Alps of New Zealand. *Science* **264,** 1434–1437 (1994).
3. Barrows, T. T., Lehman, S. J., Fifield, L. K. & DeDeckker, P. Absence of cooling in New Zealand and the adjacent ocean during the Younger Dryas chronozone. *Science* **318,** 86–89 (2007).
4. Singer, C., Shulmeister, J. & McLea, W. Evidence against a significant Younger Dryas cooling event in New Zealand. *Science* **281,** 812–814 (1998).
5. Ackert, R. P. *et al.* Patagonian glacier response during the late glacial–Holocene transition. *Science* **321,** 392–395 (2008).
6. Moreno, P. I. *et al.* Renewed glacial activity during the Antarctic cold reversal and persistence of cold conditions until 11.5 ka in SW Patagonia. *Geology* **37,** 375–378 (2009).
7. Schaefer, J. M. *et al.* High-frequency Holocene glacier fluctuations in New Zealand differ from the northern signature. *Science* **324,** 622–625 (2009).
8. Chiang, J. C. H. The Tropics in paleoclimate. *Annu. Rev. Earth Planet. Sci.* **37,** 263–297 (2009).
9. Anderson, R. F. *et al.* Wind-driven upwelling in the Southern Ocean and the deglacial rise in atmospheric CO_2. *Science* **323,** 1443–1448 (2009).
10. Jouzel, J. *et al.* A new 27 ky high resolution East Antarctic climate record. *Geophys. Res. Lett.* **28,** 3199–3202 (2001).
11. Rasmussen, S. O. *et al.* A new Greenland ice core chronology for the last glacial termination. *J. Geophys. Res.* **111,** D06102 (2006).
12. Brauer, A., Haug, G. H., Dulski, P., Sigman, D. M. & Negendank, J. F. W. An abrupt wind shift in Western Europe at the onset of the Younger Dryas cold period. *Nature Geosci.* **1,** 520–523 (2009).
13. Severinghaus, J. P., Sowers, T., Brook, E. J., Alley, R. B. & Bender, M. L. Timing of abrupt climate change at the end of the Younger Dryas interval from thermally fractionated gases in polar ice. *Nature* **391,** 141–146 (1998).
14. Denton, G. H., Alley, R. B., Comer, G. C. & Broecker, W. S. The role of seasonality in abrupt climate change. *Quat. Sci. Rev.* **24,** 1159–1182 (2005).
15. Yuan, D. *et al.* Timing, duration, and transitions of the last interglacial Asian monsoon. *Science* **304,** 575–578 (2004).
16. Lea, D. W., Pak, D. K., Peterson, L. C. & Hughen, K. A. Synchroneity of tropical and high-latitude Atlantic temperatures over the last glacial termination. *Science* **301,** 1361–1364 (2003).
17. Wang, X.-F. *et al.* Wet periods in northeastern Brazil over the past 210 kyr linked to distant climate anomalies. *Nature* **432,** 740–743 (2004).
18. Turney, C. S. M., McGlone, M. S. & Wilmshurst, J. W. Asynchronous climate change between New Zealand and the North Atlantic during the last deglaciation. *Geology* **31,** 223–226 (2003).
19. Hajdas, I., Lowe, D. J., Newnham, R. M. & Bonani, G. Timing of the late-glacial climate reversal in the Southern Hemisphere using high-resolution radiocarbon chronology for Kaipo bog, New Zealand. *Quat. Res.* **65,** 340–345 (2006).
20. Vandergoes, M. J. Dieffenbacher-Krall, A. C., Newnham, R. M., Denton, G. H. & Blaauw, M. Cooling and changing seasonality in the Southern Alps, New Zealand during the Antarctic Cold Reversal. *Quat. Sci. Rev.* **27,** 589–601 (2008).
21. Putnam, A. *et al.* In situ cosmogenic ^{10}Be production-rate calibration from the Southern Alps, New Zealand. *Quat. Geochronol.* **5,** 392–409 (2010).
22. Chinn, T. J., Winkler, S., Salinger, M. J. & Haakensen, N. Recent glacier advances in Norway and New Zealand; a comparison of their glaciological and meteorological causes. *Geogr. Ann.* **87A,** 141–157 (2005).
23. Anderson, B. & Mackintosh, A. Temperature change is the major driver of late-glacial and Holocene fluctuations in New Zealand. *Geology* **34,** 121–124 (2006).
24. Carter, L., Manighetti, B., Ganssen, G. & Northcote, L. Southwest Pacific modulation of abrupt climate change during the Antarctic Cold Reversal-Younger Dryas. *Palaeogeogr. Palaeoclimatol. Palaeoecol.* **260,** 284–298 (2008).
25. Blunier, T. J. *et al.* Timing of the Antarctic cold reversal and the atmospheric CO_2 increase with respect to the Younger Dryas event. *Geophys. Res. Lett.* **24,** 2683–2686 (1997).
26. Broecker, W. S. in *Ocean Circulation: Mechanisms and Impacts* (ed. Schmittner, A., Chiang, J. C. H. & Hemming, S. R.) 265–278 (Geophys. Monogr. Ser. 173, American Geophysical Union, 2007).
27. Timmermann, A. *et al.* The influence of a weakening of the Atlantic meridional overturning circulation on ENSO. *J. Clim.* **20,** 4899–4919 (2007).
28. Birkeland, P. W. Subdivision of Holocene glacial deposits, Ben Ohau Range, New Zealand, using relative-dating methods. *Geol. Soc. Am. Bull.* **93,** 433–449 (1982).
29. EPICA. community members. Eight glacial cycles from an Antarctic ice core. *Nature* **429,** 623–628 (2004).
30. Lemieux-Dudon, B. *et al.* Consistent dating for Antarctic and Greenland ice cores. *Quat. Sci. Rev.* **29,** 8–20 (2010).

Supplementary Information is linked to the online version of the paper at www.nature.com/nature.

Acknowledgements We thank the Comer family and W. Broecker for their support of our work. We thank B. Goehring for assisting with probability plots, S. Kelley for field assistance, T. Ritchie and K. Ritchie at Lake Ruataniwha Holiday Park for hospitality and the Helicopter Line at Glentanner Park. This research is supported by the Gary C. Comer Science and Education Foundation, the National Oceanographic and Atmospheric Administration (specifically support to G.H.D. and for field work), and National Science Foundation awards EAR-0745781, 0936077 and 0823521. D.J.A.B. was supported by Foundation for Research, Science and Technology contract CO5X0701. This is LDEO contribution #7371.

Author Contributions G.H.D., M.R.K. and J.M.S. instigated this research. M.R.K., J.M.S., R.C.F. and R.S. were responsible for all laboratory efforts, including sample processing, and data interpretation. M.R.K., A.E.P. and A.M.D. participated in field work and designed the field sampling strategies. D.J.A.B., T.J.H.C. and B.G.A. were mainly responsible for the mapping, glacier reconstructions and ELA estimates. All authors contributed to manuscript preparation.

Author Information Reprints and permissions information is available at www.nature.com/reprints. The authors declare no competing financial interests. Readers are welcome to comment on the online version of this article at www.nature.com/nature. Correspondence and requests for materials should be addressed to M.R.K. (mkaplan@ldeo.columbia.edu).

Supplementary Methods, Discussion, Tables, and Figures

I. Rationale for choosing the Irishman Stream basin for paleoclimate study (Figs. S1,S2)

We selected the Irishman basin for study after careful mapping and examination of valleys across the Southern Alps[1]. Our reasons for selecting this valley included the following:

1) The former glacier was relatively small and therefore likely to have been sensitive and responsive to climate change;

2) The moraines lie at relative high altitude, between 1780 and ~2060 m, and record past changes in atmospheric conditions well above sea level. The cirque sits in an open setting near the crest of a mountain range and thus lies in the main air stream (i.e., not perturbed by valley topography) over the central Southern Alps. As the Irishman basin is located just downwind of the most glacierized sector of the Alps, it was affected by the same (and hence is representative of the same) regional atmospheric conditions as other nearby glaciers;

3) The geometry of the former glacier was relatively simple. An essential point is that there were no independent tributaries that fed 'outside' ice into the basin (Fig. S1a), which would have introduced complications in overall glacier response and behavior;

4) The geometry of the valley is simple. The valley floor is broad and there are no major changes in the width or topography of the floor between the inner and outer moraines. The relatively

simple topographic geometry was recognized as making this basin ideal for reconstructing the former glacier and associated snow lines (Fig. S3);

5) There are no thick unconsolidated deposits that could have been molded by the glacier to change the valley geometry, or influence basal dynamics in a major way, over the relative short (10^3 yrs) time period spanning the formation of the moraine belts. The lack of thick deposits, in a basin where there is no outwash train, means that all of the material carried by the glacier are still in the basin. Ice-smoothed bedrock with relatively thin (~10^0 to ~10^1m) till veneers characterizes the basin floor;

5) There are no large mountains overshadowing the basin that could have produced a major shading effect on mass balance for a glacier terminating at one or other of the moraine positions;

6) The well-preserved arcuate cirque headwall lacks any major concave indentations. The absence of such indentations indicates that no large landslides have likely fallen into the basin. Furthermore, the dominance of smoothed bedrock and thin till veneer in the basin (i.e., no voluminous tills) also supports a lack of major amounts of landslide material onto the glacier;

7) The geometry of the valley means that, aside from small ponds, no large glacier-retreat lakes have existed. Thus, the Irishman glacier has been free of the dynamic effects of floating or calving ice that characterize some larger, low-gradient valley glaciers;

8) The major stream flows within a narrow single-thread channel. Thus, the moraines show minimal modification due to fluvial erosion or sedimentation (Figs. S1, S2);

9) There is an exceptionally well preserved record of moraine crests. The glacier history is distinctive, i.e., with several moraines preserved, because the glacier terminus was situated in a flattish part of the valley during the time in question.

Thus, careful effort went into selecting this field site and for the above reasons we assume that fluctuations of this former glacier sample the regional climate of the Southern Alps. The above list of favorable characteristics is a rare combination and is matched by few other valleys in the Southern Alps. A fortuitous combination of topography and glacier history led to the well preserved moraine record in Irishman basin, in the general absence of attributes that could have introduced 'non-climatic' complications into the proxy record. For comparison, other, locations in New Zealand where moraines of late-glacial age have been documented and dated do not have the topographic simplicity or level of moraine preservation of the Irishman basin, in particular for glacier and snow line reconstructions. And, regionally, the mountains of Australia did not intersect late-glacial snow lines (e.g., ref. 2).

II. Materials and Methods

Geologic and geomorphic setting

New Zealand is situated in the southwest Pacific region and its temperate climate reflects the interaction of sub-tropical and sub-polar air and water masses. The Southern Alps form a 500 km long barrier to the prevailing westerlies, creating an orographic precipitation regime. Mean annual precipitation rises rapidly from 3,000 mm at the seaward edge of the narrow western coastal plains to a maximum of at least 10,000 mm in the western part of the Alps close to the Main Divide. From there, precipitation diminishes approximately exponentially to about 1,000 mm in the eastern ranges[3] including around the Irishman basin.

Our mapping is in general agreement with that of prior studies[4,5], although we place more emphasis on the geomorphic expression of moraine ridges (Fig. 1). Previously, ages were estimated using relative-age methods, such as rock weathering rinds and quartz-vein heights (*see*

Geologic sources of error). However, we have the advantage of a new and precise chronometer, in-situ produced ^{10}Be. Our dating shows that moraines in Irishman basin previously inferred to be of mid- to late Holocene in age[4,5] are actually late-glacial to earliest Holocene (Fig. 1). Down-valley of the 'outer moraine belt' (e.g., Fig. S1) lies a generally smooth basin floor, with a poorly preserved ridge, partly buried by scree on the true left side of the basin. We refer to this area of smooth ground and the poorly preserved ridge as the 'outboard moraine' (Fig. 1). McGregor[4] and Birkeland[5] inferred a late-glacial age for the poorly preserved ridge. By their criteria and assessment this implied that they considered it to be substantially older than the well defined moraines documented here. As these moraines are now documented to be late-glacial in age, the outboard moraine ridge may thus be older, possibly closer in age to LGM, given the substantial differences in weathering characteristics and preservation[4,5].

The ^{10}Be samples came from large boulders embedded in the crests of discrete moraine ridges, except for IS-06-29, and -30 and -49. Of these, the two large isolated boulders that provided samples IS-06-29 and 30 lie down-valley of the outer moraine belt, within the smooth outboard moraine area. The modes of emplacement of these boulders and their geomorphic significance are not clear, given they are not on a moraine ridge. Possibilities include that they were deposited by ablating ice, that they are the products of rock fall from the nearby valley side or that they rolled off the late-glacial ice snout down-valley (their ages are statistically indistinguishable from those on the outer moraine belt). The latter, IS-06-30, is relatively closer to the scree-covered valley wall and has a steeply sloping side that was sampled. The top of boulder IS-06-29 is also relatively eroded compared with most other samples (see *Geologic sources of error*). We note also that IS-06-49 is a prominent embedded boulder relatively far

from valley walls and located close to a small remnant moraine ridge. However, it is encircled by alluvial fan material (Fig. 1), the emplacement of which may have affected its exposure history.

Interpretation of moraine records

The temperate environmental setting of South Island glaciers means that they respond sensitively to small changes in climate, especially temperature (<0.5°C)[6-9], as they are not 'precipitation-limited.' Small, geometrically simple, glaciers are likely to equilibrate rapidly (e.g. of the order of years) to a shift in climate. Thus, we assume that lateral or terminal moraine ridges have been constructed at times when a glacier was in, or close to, equilibrium with prevailing climate. Surface sediments on a moraine ridge represent the culmination of its construction and we assume that the construction ceased due to withdrawal of the glacier from that position. Thus, we regard the surface exposure age of a boulder on a moraine ridge as a close approximation of the time when the glacier withdrew from that ridge.

Sampling and field protocols

We sampled large boulders composed of a Mesozoic-age, hard, quartzo-feldspathic, fine-grained greywacke sandstone. Many of the boulders contain fracture-fill quartz veins of various thicknesses (Fig. S2). Samples were taken from the upper 1-3 cm from the most stable-looking flattish section, and if possible the center, of the boulder's top surface. Samples were collected with either hammer and chisel or a drill. The azimuthal elevations of the surrounding landscape were measured using a compass and clinometer. We used a Trimble ProXH GPS system relative to the WGS 1984 datum to measure position including altitudes. All measurements were corrected differentially using continuous data collected by the Mt. John Observatory base station

(MTJO; latitude: −43.985706, longitude: 170.464943, height above ellipsoid: 1043.660 m; height above mean sea level relative to the tide-gauge data at Lyttelton, New Zealand: 1037.46 m). Post-processed uncertainties (1σ) ranged from 0.2 to 0.7 m, and 0.2 to 1.2 m, for latitude-longitude and altitudes, respectively, for all sample sites.

Cosmogenic ^{10}Be measurements

All samples were processed at the cosmogenic dating laboratory at the Lamont-Doherty Earth Observatory (LDEO). Samples were measured, described and photographed before crushing to 125 μm–710 μm. We followed geochemical processing protocols as explained in ref. 10 and at LDEO_Cosmogenic_ Nuclide_Lab/Chemistry.html. In Figure S4 we present different statistical central tendencies, i.e., mean, median, and associated errors, which notably provide the same result. For the arithmetic mean ages of the moraines, we choose to present a conservative error, i.e., including that for the analytical AMS measurement and the production rate.

Three recent developments enable unprecedented accuracy in the ^{10}Be dating of late-glacial moraines in New Zealand (see ref 10). First, a local production rate is utilized and thus systematic uncertainties that have plagued prior studies are reduced (see *Local production rate and other systematic sources of error,* below). Second, a 'custom-made' low process blank made from a deep mine beryl crystal allows preparation and measurement of samples as few as ~10^3 atoms of ^{10}Be per gram with ^{10}Be/^{9}Be ratios >1x10^{-14}. The process blanks measured with the samples presented in Table S1 afforded ^{9}Be/^{10}Be measurements between 5 x10^{-16} and 20x10^{-16} corresponding to between 6,000 and 26,000 ^{10}Be atoms/g. The low background blank allows smaller samples (i.e., faster processing) and efficient removal of all material except ^{10}Be in the chemical procedures, resulting in high AMS currents and precise measurements. We spiked all

samples with 0.2 mg of the ^{9}Be carrier (concentration = 996 ppm). Third, recent developments at the Center of Accelerator Mass Spectrometry at Lawrence Livermore National Laboratory (LLNL) make it possible to measure low ^{10}Be concentrations. A custom-designed ion source produced high ^{9}Be ion currents ranging from 12 to 21 uA (mean of ~18 uA) for the samples presented in Table S1, and yielded ^{10}Be measurements of typically <3% (1σ). Such precision also allows better comparison than previously possible of successive glacial events close in time in the same area, such as between the outer moraine belt and inner part of Irishman basin. All input parameters needed to calculate the ^{10}Be ages discussed in this paper are given in Table S1.

Local production rate and other systematic sources of error

Typically, the major sources of systematic error relate to the production rate value and scaling schemes used to calculate cosmogenic ages. In contrast to previous ^{10}Be-based studies such as on South Island and elsewhere in the Southern Hemisphere (e.g., in ref 11,12), we minimize the systematic uncertainties by using a newly-established, high-precision ^{10}Be production rate from Macaulay valley, ~60 km northeast of Irishman basin[13]. This production rate was tested nearby, ~7 km southeast of the Irishman basin, on independently-dated moraines ~800 m in elevation at Boundary Stream. Utilizing the generally accepted global production rate[14,15] yielded ^{10}Be ages at Boundary Stream that are inconsistently young compared to the independent ^{14}C age control. In contrast, the Macaulay-South Island production rate provided ^{10}Be ages that agree with the ^{14}C data[13]. The local production rate in New Zealand is ~12 to 14% lower than the global production rate summarized in refs 14 and 15, but similar to that documented in ref. 16.

In Table S2, we provide ages according to the different currently accepted scaling schemes. Existence of a local production rate also reduces the differences between scaling schemes, mainly to an elevation influence[15], as the variability due to latitude and longitude on central South Island is minimal. However, we discuss ages in this paper based on the 'Lm' scaling scheme[15] for two reasons. First, and most important, the 'best fit' between the ^{14}C and ^{10}Be data at the nearby Boundary Stream and Macaulay sites is achieved with the 'Lm' scaling scheme[13]. Second, for consistency between this and other Southern Hemisphere studies (which used the non-local production rate in ref. 14,15)[11,12] we use 'Lm'. Nonetheless, age differences depending on the scaling scheme do not affect the main conclusions drawn here.

We also highlight that when comparing relative ages of adjacent moraines, e.g., within Irishman basin, systematic uncertainties can be ignored because spatial differences are negligible.

Geologic sources of error

Near-surface geologic and geomorphic processes may lead to erroneous apparent surface exposure ages. For example, a boulder may contain ^{10}Be inherited from prior exposure to cosmic radiation, either in-situ in its original outcrop or due to reworking from a previous surficial deposit. Inheritance is typically indicated by anomalies in the age distributions, or by the presence of significantly older age outliers. Geomorphic processes may also produce boulder ages that are younger than the time of deposition. For example, after a glacier retreated, a boulder may have moved due to melting of buried ice, or a boulder may have been deposited after formation of the moraine, by nonglaciogenic processes, such as rockfall. Other processes that may produce exposure ages that are younger than the true age of the moraine include boulder surface erosion, snow-cover (see below), and post-depositional exhumation.

The greywacke lithology is relatively resistant to weathering on the short time scales considered here, particularly where annual precipitation volumes are relatively small. We assume the erosion of the sampled surface to be minimal over the time-scales discussed here (excluding perhaps two 'young outliers' at 2σ; IS-06-16 and 17; see below). This assumption is supported by the relative relief of quartz veins that stand above the surfaces that we sampled. On all boulders sampled, quartz vein heights were measured. These veins typically are less 3 mm high and provide a minimum value for the amount of erosion since emplacement of the boulder, of less than 0.3 cm over >10,000 years. These quartz vein heights are consistent with data from Birkeland[5] (2.59±0.86 to 4.3±1.32 mm) especially in light of the fact that we avoided boulders and surfaces that had obvious erosion and chose the most stable part of the top. Erosion rates of 0.3 mm/kyr would result in measured ages that underestimate the emplacement ages by <0.3%. Nonetheless, we highlight that all ages are presented as zero-erosion ages and this uncertainty does not affect our conclusions.

Effects of such geologic or geomorphic processes appear to be minimal in the Irishman basin study area. Moraine ages are exceptionally consistent, even given <3% analytical errors, and there are only three outliers at >2σ, all in the NE area of the basin (IS-06-16, 17, 20). The outer moraine belt and inner moraine belts A and B provide coherent age distributions (Fig. S4), and each has mean and median ages that coincide. The standard deviation of the mean ages of each moraine set is similar to the individual age error (analytic) and the reduced chi-squared (χ^2) values are close to 1, indicating that the samples may be regarded as a single population and that the analytical errors alone may account for the age scatter[17].

In this middle latitude setting, where ice was likely warm-based, inheritance relative to the analytical precision is not apparent, as it should be uniquely different for each sample. A

notable exception in this study is sample (IS-06-20) which affords an age more than 2σ different than all other ages. The sampled face of this boulder was most likely formerly exposed in a rock outcrop, given its position relatively close to the headwall, before the late-glacial period. Two samples provide ages that are >2σ different (less) than other sample ages on their respective moraines, IS-06-16 and IS-06-17. The former sample was re-measured, which confirmed the anomalously young exposure age obtained at first measurement. Post-depositional erosion or exfoliation of the boulder surfaces is a likely explanation.

The Irishman basin lies above the elevation (~1500 m) at which snow lies persistently during the winter months in the Southern Alps. This raises the possibility that seasonal snow cover may have affected the exposure to cosmic radiation on the tops of boulders on moraine crests in Irishman basin. We outline three points of information. First, the winter snow pack in this part of the Southern Alps, judging from nearby skifield measurements over the last few decades, has rarely been thicker than 2 m or so, and at such thicknesses persists at most for a few months. Second, we over-flew the Irishman basin area on 22 August 2009 in order to inspect the snow cover. At that time of year (austral late winter), seasonal snow is typically at its maximum and 2009 was notable for thicker than usual snow cover. We observed that boulders on moraine crests, including many of those sampled, stood out prominently from the snow blanket (also see Fig. S1a). Third, the coherence of the age distributions, especially given 1σ uncertainties typically <3% (300 years, Table S2) does not reveal any notable effect, as would be expected from episodic attenuation of cosmic radiation due to a differential thickness of snow cover, on sampled boulders having varying heights and top shape-sizes.

A lack of knowledge of snow conditions prior to recorded observations (in New Zealand, the last 150 years at most) leaves no option other than to extrapolate modern observations back

into the past. We thus assume that on average over the Holocene, 2 meters of snow may have covered the ground for 4 months of the year. The heights of the boulders range from about ~1 to 4 meters, with most sides of most blocks between 1 and 3 m high. Assuming 2 m of snow from the ground up, and a draping over the landscape, this means that boulders could have had ~1 meter of snow on top surfaces or much less; many boulder top flat surfaces, where sampled, are small in area (~50 cm across) and would not sustain relatively thick 'top-hat scenarios' of snow cover (e.g., see Fig S2). In depressions, more than 2 meters is expected to collect during winter, but all samples are from moraine crests, and the boulders sit on top of the crests (except IS-06-29 and 30, and 49). Assuming a maximum of 1 m of snow (density of <0.3gm/Kg) for 4 months of the year increases the ages by <2.9%. The existence of 50 cm of snow for 4 months increases the ages by <1.3%. Given the uncertainty as to whether or not any correction is even needed, we prefer not to introduce any speculative minor adjustments for snow cover. We note that for the ages ranges discussed here, the worst case of ~2 m of snow on the ground and ~1 m on every boulder top implies age increases of between 300 and 400 years, which do not alter the main conclusions of this paper.

II. Glacier surface area, distance of retreat, and snow lines

Reconstructions of the former glacier extents are presented in Figure S3, along with derived former snow line elevations (Equilibrium Line Altitudes). We have reconstructed the glacier as it was at the completion of formation of the outer moraine belt and at inner moraine belt A. In addition we illustrate the ice retreat distance between these two positions. Data are summarized in Table S3. Glacier lengths were measured from the outer moraine belt, back up-

valley. The emphasis in this study is on the pattern of change for these parameters, between ~13 and 11.5 kyr ago.

Glacier and paleo snow line reconstructions (Fig. S3)

We reconstructed the glacier surface dimensions using the following procedure:

1) Glacier extent: downstream ice limits are defined precisely by terminal moraines where they are preserved. Maximum upstream limits are defined by the catchment head. We have made 'larger volume ice models' (Fig. S3 a,b) where the upstream glacier margin extends to the catchment head. In addition we have constructed 'smaller volume ice models' where the upstream limit runs closer to the ~bases of steep bluffs around the catchment headwall (Fig. S3 c,d) and the right lateral margin follows the rock glacierized landforms on the west side of the basin for a short distance, assuming they were the former right lateral moraines. The upper limit of the glacier at the headwall, which affects the total glacier area, remains relatively constant as glacier area changes, as the topographic factors controlling the uppermost part of the accumulation limit change little. Thus, changes in placement along the uppermost approximately vertical headwall have little effect on our reconstructions at different times for each respective ice model (S3a-d);

2) Glacier surface elevations: where present day topographic contours cross former ice margin, they define to close precision the elevation of that ice margin. Such areas are illustrated in Figure S3 as 'height control', and these provide the most robust controls on glacier surface reconstruction. From these points of control, paleo-contours are inferred on the ice surfaces using a variety of considerations. Least ambiguous are where paired

control points exist on opposite margins, such as the outer moraine belt between 1780 and 1860 m. The terminus of inner moraine belt intersects contours between 1880 and 2000 m. These points of control define the glacier surface gradients in the lower reaches of the ice tongue (Fig. S3 a,b). The ice gradients provide a starting framework for extrapolating the ice surface up-valley. Ice flow is approximately downhill and we employ the principle that ice surface topographic contours (isolines) are always normal to the flow vectors (flowlines). The flowlines typically converge above the ELA and diverge in the ablation area[18]. Except where there may be obvious irregularities that would have been salient above the ice surface, an assumption of at least 20 m ice thickness has guided the 'larger ice volume model' reconstruction. This model is also directly constrained by the headwall topographic contours, which define ice surface elevations there. Caution was exercised in places where the basin floor (i.e. former glacier bed) has been modified by subsequent deposition, via younger moraines, screes or rock glacier debris. The reconstructed glaciers had no major source tributaries entering Irishman basin or calving margins, to consider. In addition, striation vectors are available at two sites (Fig. S3a). The reconstructed glaciers, isolines and flowlines are all illustrated in Figure S3;

3) We then calculated the cumulative area of ice within the 1900, 2000, 2100, and 2200 m, and the uppermost limit of surface contours (Table S3; Fig. S3e-f);

4) Equilibrium Line Altitude (ELA), commonly called 'snow line,' was estimated from the area versus altitude delineations (Fig. S3e-f). The universal average accumulation to ablation area (AAR) ratio of 2:1 or 0.67/0.33 is used here[19]. ELA values in Irishman basin are for a south-southwest facing aspect[19];

5) As our elevation control is derived from the 20-m topographic contours mapped photogrammetrically, we place an indicative ±20 m error on each ELA estimate. The difference in ELA is thus assigned an indicative error of ±40 m.

Of the models presented, we regard the 'larger ice volume' models as maximum estimates of ice tongues in this basin. The 'smaller ice volume' models are perhaps characteristic of how small a glacier could be in order to form the observed moraines (cf., ^{10}Be ages on moraine surface boulders). Most important, in this study we emphasize the increase in ELA from the 13 kyr outer moraine belt to the inner moraine belt A (e.g., in Fig. 1), which is similar (~70-80 m), whether the minimum or maximum reconstructions are used. An alternative possibility is that the best working estimate of ELA is the median of each model for each respective glacier extent. This would equate the outer moraine belt with an ELA of 1965 m and inner moraine belt A with an ELA of 2040 m. Taking the above ELA values, along with the effects of slope aspect on ELA[19], we have drawn the approximate extent of the accumulation versus ablation areas in Figures S3a-d. This subdivision equates well with the AAR of 0.66 assumed in these reconstructions.

We have two lines of ground truthing for our ELA estimates. First, the maximum elevation of the lateral moraine deposits is a minimum for the ELA of the glacier that formed the moraine. The approximate maximum elevations of preserved lateral moraines are 1900 and 2000 m, respectively, for the outer moraine belt and inner moraine belt A. Second, the difference in elevations of the termini is a broad maximum for the difference in ELA at the times each moraine formed. The difference in terminal elevations (Fig. S3) is 1780±20 compared with

1850±20 m. Our estimate of the ELA change of ~75±40 m (or 70-80±40) is compatible with both these considerations.

The two prominent inner moraine belts A and B are immediately adjacent to one another (Figs. 1, S1, and S2) and the ELA on inner moraine belt B must have been only slightly higher than that of inner moraine belt A. There is insufficient geomorphic or elevation control to attempt a meaningful reconstruction of the inner moraine belt B glacier extent relative to that of inner moraine belt A. The difference in their terminal elevations is approximately 30 m, and this provides a broad maximum for the difference in their ELAs. Alternatively, extrapolation of ELA, based on <100 m of additional retreat from the outer moraine belt and inner moraine belt A leads to an estimated increase of ~10 m.

Innermost moraine sequence and the modern snow line

In Figure 2, panel a, the <11.5 kyr ago retreat distance and ELA values are shown as dashed lines for ~500 years. We simply assume an average retreat rate from 11.5 kyr ago until present for the short distance to the headwall. However, we highlight that this study focuses on the time period 13 to 11.5 kyr ago, and the precise nature of snow line change after this interval does not affect the main conclusions. The chronology here indicates that after 11.5 kyr ago, the margin did not readvance to this position during the Holocene. The few moraines preserved farther inboard were suggested in ref 5 to be late Holocene. However, our high-precision dating has shown that earlier estimates using relative-dating methods should be regarded as minima for the time of deposition. We note that the innermost moraines near the headwall lie adjacent to, and locally have been disrupted by, large, complex rock glaciers, and are flanked by extensive

scree. Thus, at least some of these innermost moraines seem to be set in an immediate landscape with some maturity of age.

No glaciers exist today in the Irishman basin catchment. The nearest modern glaciers are 5 km away to the northwest. During fieldwork, we noted that permanent snow and ice patches persist under the cirque headwall in the northwest part area, starting at ~2260 m, through the summer. The lack of an observed modern permanent snow line in Irishman basin prevents the estimation of late-glacial snow line depression relative to present snow line. For comparison, a general snow line elevation trend surface for the Southern Alps[19,20] predicts that over Irishman basin the modern ELA should be about or greater than 2200 m. Past snow line gradients though may not have been parallel to that at present over the Ben Ohau range. We reiterate that our study focuses on the time period 13 to 11.5 kyr ago, and our conclusions are not affected by the precise nature of present ELA.

Table S1. Geographical and analytical data for the samples from Irishman basin

Sample	Lat. (°S)	Long. (°W)	Elev (m a.s.l.)[a]	Thickness (cm)	Topographic Shielding	^{10}Be (atoms gm^{-1})	^{10}Be/^{9}Be ratio standard
Outer part of Irishman basin							
IS-06-31	-43.9985	170.0394	1817	1.11	0.983	253,696 ± 6,026	3.15E-12
IS-06-32	-43.9984	170.0401	1820	2.65	0.995	251,833 ± 6,778	3.15E-12
IS-06-33	-43.9983	170.0401	1820	3.88	0.995	217,902 ± 4,692	2.85E-12
IS-06-35	-43.9985	170.0383	1809	1.40	0.992	239,869 ± 5,697	3.15E-12
IS-06-36	-43.9986	170.0372	1797	1.10	0.994	211,444 ± 4,191	2.85E-12
IS-06-37	-43.9985	170.0377	1804	3.64	0.988	233,155 ± 5,533	3.15E-12
IS-06-38	-43.9967	170.0358	1816	3.40	0.991	233,809 ± 5,551	3.15E-12
IS-06-39	-43.9968	170.0358	1815	2.16	0.992	240,888 ± 5,712	3.15E-12
IS-06-40	-43.9975	170.0357	1810	0.96	0.994	214,422 ± 5,081	2.85E-12
IS-06-41	-43.9975	170.0389	1803	2.38	0.992	235,223 ± 5,514	3.15E-12
IS-06-42	-43.9975	170.0391	1804	2.15	0.993	235,406 ± 5,519	3.15E-12
IS-06-43	-43.9969	170.0383	1803	0.63	0.990	202,065 ± 5,838	2.85E-12
IS-06-44	-43.9967	170.0396	1808	2.11	0.988	219,044 ± 3,952	2.85E-12
IS-06-29	-43.9993	170.0381	1809	1.67	0.993	234,510 ± 5,520	3.15E-12
IS-06-30	-43.9998	170.0384	1807	2.30	0.993	233,739 ± 5,524	3.15E-12
Inner part of Irishman basin							
IS-06-15	-43.9919	170.0491	2001	2.59	0.973	234,429 ± 5,413	2.85E-12
IS-06-16[b]	-43.9919	170.0491	1999	1.99	0.989	139,381 ± 2,956	2.85E-12
IS-06-16[b]	-43.9919	170.0491	1999	1.99	0.989	139,331 ± 3,649	2.85E-12
IS-06-17	-43.9901	170.0512	2016	2.77	0.983	198,061 ± 4,543	2.85E-12
IS-06-18	-43.9901	170.0513	2015	3.07	0.981	231,801 ± 6,781	2.85E-12
IS-06-19	-43.9905	170.0505	2006	1.89	0.988	229,467 ± 4,796	2.85E-12
IS-06-20	-43.9904	170.0495	2003	2.98	0.988	345,737 ± 7,951	2.85E-12
IS-06-21	-43.9900	170.0479	2004	1.91	0.988	226,377 ± 5,251	2.85E-12
IS-06-22	-43.9900	170.0475	1994	2.78	0.988	239,078 ± 5,773	3.15E-12
IS-06-23	-43.9902	170.0473	1982	1.57	0.987	231,041 ± 5,563	3.15E-12
IS-06-24	-43.9906	170.0475	1981	2.53	0.991	236,520 ± 5,464	2.85E-12
IS-06-25	-43.9909	170.0468	1955	2.67	0.986	245,617 ± 5,340	3.15E-12
IS-06-26	-43.9908	170.0450	1917	3.15	0.982	202,443 ± 5,155	2.85E-12
IS-06-27	-43.9908	170.0443	1905	4.44	0.984	207,131 ± 5,262	2.85E-12
IS-06-28	-43.9916	170.0443	1878	2.72	0.984	206,810 ± 5,865	2.85E-12
IS-06-47	-43.9917	170.0421	1850	1.13	0.984	229,365 ± 5,471	3.15E-12
IS-06-49	-43.9926	170.0422	1844	1.05	0.980	220,185 ± 5,207	3.15E-12
Near NE headwall							
IS-06-01	-43.9905	170.0505	2006	1.89	0.988	229,467 ± 4,796	2.85E-12
IS-06-02	-43.9906	170.0475	1981	2.53	0.991	236,520 ± 5,464	2.85E-12
IS-06-03	-43.9909	170.0468	1955	2.67	0.986	245,617 ± 5,340	2.85E-12

Note: Four procedural blanks in total (^{10}Be/^{9}Be = (0.3– 2)*10^{-15}), consisting of 0.2 ml of ^{9}Be carrier, were processed identically to the samples, with one accompanying each sample batch, respectively (4 batches in total). Standards used for normalization: 3.15^{-12} = KNSTD3110; 2.85^{-12} = 07KNSTD3110. Shown are 1σ analytical AMS uncertainties.

[a]Measured with a Trimble GPS system.

[b]IS-06-16 was measured twice.

Table S2. ^{10}Be ages from Irishman basin

Sample	Lm	int	ext	Du	int	ext	Li	int	ext	De	int	ext
Outer part of Irishman basin												
IS-06-31	13700 ±	330	440	13200 ±	310	420	13200 ±	320	410	13300 ±	320	420
IS-06-32	13500 ±	370	470	13000 ±	350	450	13100 ±	350	430	13100 ±	350	450
IS-06-33	13100 ±	280	400	12600 ±	270	380	12600 ±	270	370	12700 ±	270	380
IS-06-35	12900 ±	310	410	12400 ±	300	390	12500 ±	300	380	12500 ±	300	400
IS-06-36	12600 ±	250	370	12200 ±	240	350	12200 ±	240	340	12300 ±	240	350
IS-06-37	12800 ±	310	410	12400 ±	300	390	12400 ±	300	380	12500 ±	300	390
IS-06-38	12700 ±	300	410	12200 ±	290	390	12300 ±	290	380	12300 ±	290	390
IS-06-39	13000 ±	310	420	12500 ±	300	400	12500 ±	300	380	12600 ±	300	400
IS-06-40	12700 ±	300	410	12200 ±	290	390	12300 ±	290	380	12300 ±	290	390
IS-06-41	12800 ±	300	410	12300 ±	290	390	12400 ±	290	380	12400 ±	290	390
IS-06-42	12800 ±	300	410	12300 ±	290	390	12300 ±	290	380	12400 ±	290	390
IS-06-43	12000 ±	350	430	11600 ±	340	420	11600 ±	340	410	11700 ±	340	420
IS-06-44	13200 ±	240	370	12700 ±	230	350	12700 ±	230	340	12800 ±	230	350
IS-06-29	12600 ±	300	400	12200 ±	290	390	12200 ±	290	370	12300 ±	290	390
IS-06-30	12700 ±	300	410	12200 ±	290	390	12200 ±	290	380	12300 ±	290	390
Inner part of Irishman basin												
IS-06-15	12500 ±	290	400	11900 ±	280	370	12000 ±	280	360	12000 ±	280	370
IS-06-16[a]	7260 ±	150	220	6970 ±	150	210	6890 ±	150	200	6960 ±	150	210
IS-06-16[a]	7260 ±	190	250	6970 ±	180	230	6890 ±	180	220	6960 ±	180	230
IS-06-17	10400 ±	240	330	9880 ±	230	310	9850 ±	230	300	9940 ±	230	310
IS-06-18	12200 ±	360	440	11600 ±	340	420	11600 ±	340	410	11700 ±	340	420
IS-06-19	12000 ±	250	360	11400 ±	240	340	11400 ±	240	330	11500 ±	240	340
IS-06-20	18100 ±	420	570	17200 ±	400	540	17300 ±	400	520	17400 ±	400	540
IS-06-21	11800 ±	280	370	11300 ±	260	350	11300 ±	260	340	11400 ±	260	350
IS-06-22	11400 ±	280	370	10900 ±	260	350	10900 ±	260	340	11000 ±	270	350
IS-06-23	11100 ±	270	360	10600 ±	260	340	10600 ±	260	330	10600 ±	260	340
IS-06-24	12600 ±	290	400	12000 ±	280	380	12000 ±	280	360	12100 ±	280	380
IS-06-25	12100 ±	260	370	11600 ±	250	350	11600 ±	250	340	11700 ±	250	350
IS-06-26	11400 ±	290	380	10900 ±	280	360	10900 ±	280	350	11000 ±	280	360
IS-06-27	11900 ±	300	400	11400 ±	290	380	11400 ±	290	370	11500 ±	290	380
IS-06-28	11900 ±	340	430	11500 ±	330	410	11500 ±	330	400	11500 ±	330	410
IS-06-47	12100 ±	290	390	11600 ±	280	370	11600 ±	280	360	11700 ±	280	370
IS-06-49	11700 ±	280	370	11200 ±	270	360	11300 ±	270	350	11300 ±	270	360
Near NE headwall												
IS-06-01	11400 ±	260	360	10800 ±	250	340	10800 ±	250	330	10900 ±	250	340
IS-06-02	9690 ±	210	300	9210 ±	200	280	9160 ±	200	270	9250 ±	200	280
IS-06-03	13300 ±	310	420	12600 ±	290	390	12700 ±	290	380	12800 ±	300	400

Note: ^{10}Be ages in years based on four different scaling protocols[15]. 'Lm' is the time dependent version of Stone/Lal scaling scheme[14]. 'Du' is based on the scaling scheme according to ref 21, 'Li' the scaling according to refs 22 and 23, and the 'De' scaling scheme is given in ref. 24. We use the new production rate locally determined at the Macaulay valley[13]. Age uncertainties include internal analytical error only (=int) and external error, including systematic uncertainties (=ext)[15] that include scaling to the latitude and altitude of Irishman basin. The discussion is based on the numbers given in the first age column (Lm) as explained in the text.

[a]Sample IS-06-16 was measured twice.

Table S3. Reconstructed glacier parameters for Irishman basin

Moraine	Age (kyr)	Retreat Distance (km)	Cum. area (km^2)[a]	ELA @ 0.66[a]	Cum. area (km^2)[b]	ELA @ 0.66[b]
Outer moraine belt	13.0 ± 0.4	0	1.973	1980	1.66	1950
Inner moraine belt A	12.2 ± 0.3	980	1.065	2050	0.66	2030
Inner moraine belt B[c]	11.5 ± 0.3	1080				*2040*

Notes: ELA=equilibrium line altitude, which is estimated using an accumulation to ablation area ratio (AAR) of 2:1 or 0.66[19]. We place an indicative ±20 m error on our respective ELA estimates. For this table, systematic uncertainties are ignored because (relative) moraine ages are compared in the same basin (Fig. S4).

[a] Estimates for maximum glacier reconstruction shown in Figure S3.

[b] Estimates for minimum glacier reconstruction shown in Figure S3 (used in Figure 2, panel A). However, we highlight that the ELA increase from the 13 kyr outer moraine belt to the inner moraine A is similar (~70-80 m), whether the minimum or maximum reconstructions are used.

[c] For inner moraine belt B, for Figure 2, extrapolation of ELA (italics) is based on ~100 m of additional retreat from the outer moraine belt and inner moraine belt A (see text).

References cited:

1. GNS Science. Central South Island Glacial Geomorphology. http://maps.gns.cri.nz/website/csigg/ (2010).
2. Barrows, T. T., Stone, J., Fifield, K. & Creswell, R. The timing of the last glacial maximum in Australia. *Quat. Science Reviews* **21**, 59-173 (2002).
3. Henderson, R. D. & Thompson, S. M. Extreme rainfalls in the Southern Alps of New Zealand. *J. of Hydrology (New Zealand)* **38**, 309-330 (1999).
4. McGregor, V. R. Holocene moraines and rock glaciers in the central Ben Ohau Range, south Canterbury, New Zealand. *J. Glaciology* **6**, 737-748 (1967).
5. Birkeland, P. W. Subdivision of Holocene glacial deposits, Ben Ohau Range, New Zealand, using relative-dating methods. *Geol. Soc. Amer. Bull*. **93**, 433-449 (1982).
6. Chinn, T. J. New Zealand glacier responses to climate change of the past century. *NZ J. Geol. Geophys.* **39**, 415–428 (1996).
7. Chinn, T.J., Winkler, S., Salinger M.J. & Haakensen, N. Recent glacier advances in Norway and New Zealand; a comparison of their glaciological and meteorological causes. *Geogr. Ann.* **87A** , 141-157 (2005).
8. Anderson, B. & Mackintosh, A. Temperature change is the major driver of late-glacial and Holocene fluctuations in New Zealand. *Geology* **34**, 121-124 (2006).
9. Anderson, B., Mackintosh, A., Stumm, D., George, L., Kerr, T., Winter-Billington, A. & Fitzsimons, S. Climate sensitivity of a high-precipitation glacier in New Zealand. *J. of Glaciology* **56**, 114-128 (2010).
10. Schaefer, J. M. *et al.* High-Frequency Holocene Glacier Fluctuations in New Zealand Differ from the Northern Signature. *Science* **324**, 622-625 (2009).

11. Barrows, T. T., Lehman, S. J., Fifield, L. K. & DeDeckker, P. Absence of cooling in New Zealand and the adjacent ocean during the Younger Dryas Chronozone. *Science* **318**, 86-89 (2007).

12. Ackert, R. P. *et al.* Patagonian Glacier Response During the Late Glacial–Holocene Transition. *Science* **321**, 392-395 (2008).

13. Putnam, A. *et al.* In situ cosmogenic ^{10}Be production-rate calibration from the Southern Alps, New Zealand. *Quat. Geochronology*, doi:10.1016/j.quageo.2009.12.001 (2010).

14. Stone, J. O. Air pressure and cosmogenic isotope production. *J. Geophys. Res.* **105**, 23753-23759 (2000).

15. Balco, G., Stone, J. O, Lifton, N. A. & Dunai, T. J. A complete and easily accessible means of calculating surface exposure ages or erosion rates from ^{10}Be and ^{26}Al measurements. *Quat. Geochronology* **3,** 174-195 (2008).

16. Balco, G., Briner, J. P., Finkel, R. C., Rayburn, J., Ridge, J. C. & Schaefer, J. M. Regional beryllium-10 production rate calibration for late-glacial northeastern North America. *Quat. Geochronology* **4**, 93-107 (2009).

17. Bevington, P. & Robinson, D. *Data Reduction and Error Analysis for the Physical Sciences*. WCB McGraw-Hill, New York, 320 pp. (1992).

18. Paterson, W. S. B. *The Physics of Glaciers.* 3rd edition. Oxford, Pergamon, ix, 480 pp. (1994).

19. Chinn, T. J. H. & Whitehouse, I. E. Glaciers snow line variations in the Southern Alps, New Zealand. In, World Glacier Inventory. *International Association of Hydrological Sciences Publication*, No. 126, 219-228 (1980).

20. Lamont, G.N., Chinn, T. J. & Fitzharris, B. B. Slope of glacier ELAs in the Southern Alps of New Zealand in relation to atmospheric circulation patterns. *Global Planet. Change* **22**, 209-219 (1999).

21. Dunai, T. J. Influence of secular variation of the magnetic field on production rates of in situ produced cosmogenic nuclides. *Earth and Planet. Sci. Lett.* **193**, 197-212 (2001).

22. Pigati, J. S. & Lifton, N. A. Geomagnetic effects on time-integrated cosmogenic nuclide production with emphasis on in situ ^{14}C and ^{10}Be. *Earth and Planet. Sci. Lett.* **226**, 193-205 (2004).

23. Lifton, N., Smart, D. & Shea, M. Scaling time-integrated in situ cosmogenic nuclide production rates using a continuous geomagnetic model. *Earth and Planet. Sci. Lett.* **268**, 190-201 (2008).

24. Desilets, D. & Zreda, M. Spatial and temporal distribution of secondary cosmic-ray nucleon intensities and applications to in-situ cosmogenic dating. *Earth and Planet. Sci. Lett.* **206**, 21-42 (2003).

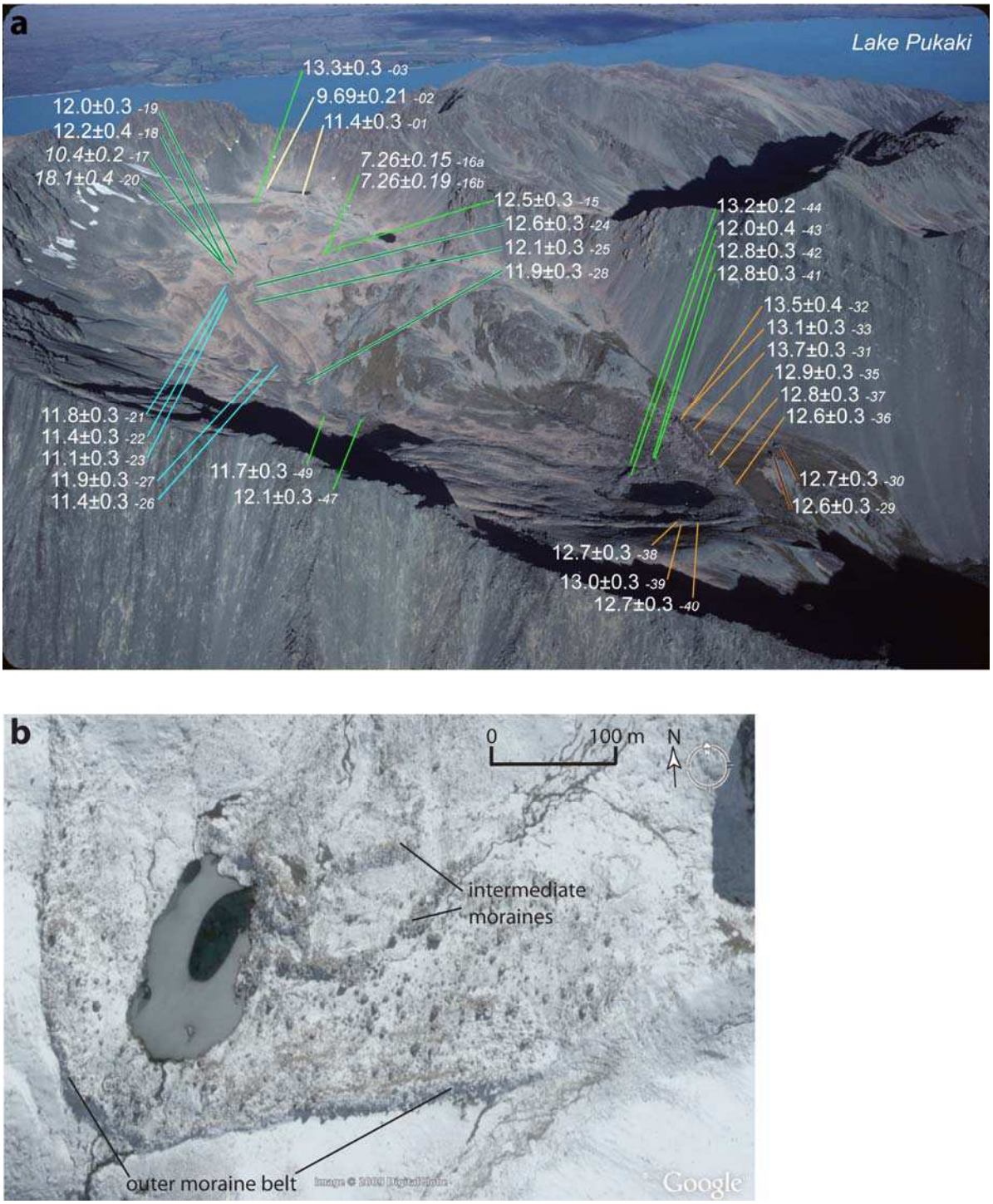

Figure S1. Images that illustrate why the Irishman Stream basin was chosen for study of paleoclimate (see text). a, A photograph that focuses on the entire Irishman basin, and the locations of all the ^{10}Be ages (Table S2, individual ages are shown with 1σ analytical error), with the last part of the *sample label* (photo: G. Denton). Color of lines matches location symbols on Figure 1. Vantage is east; **b,** Google Earth image of the outer part of Irishman basin. The figure highlights the well preserved morphology of the late-glacial moraine (outer moraine belt) in this part of the Ben Ohau Range, which specifically led us to target it for ^{10}Be analyses.

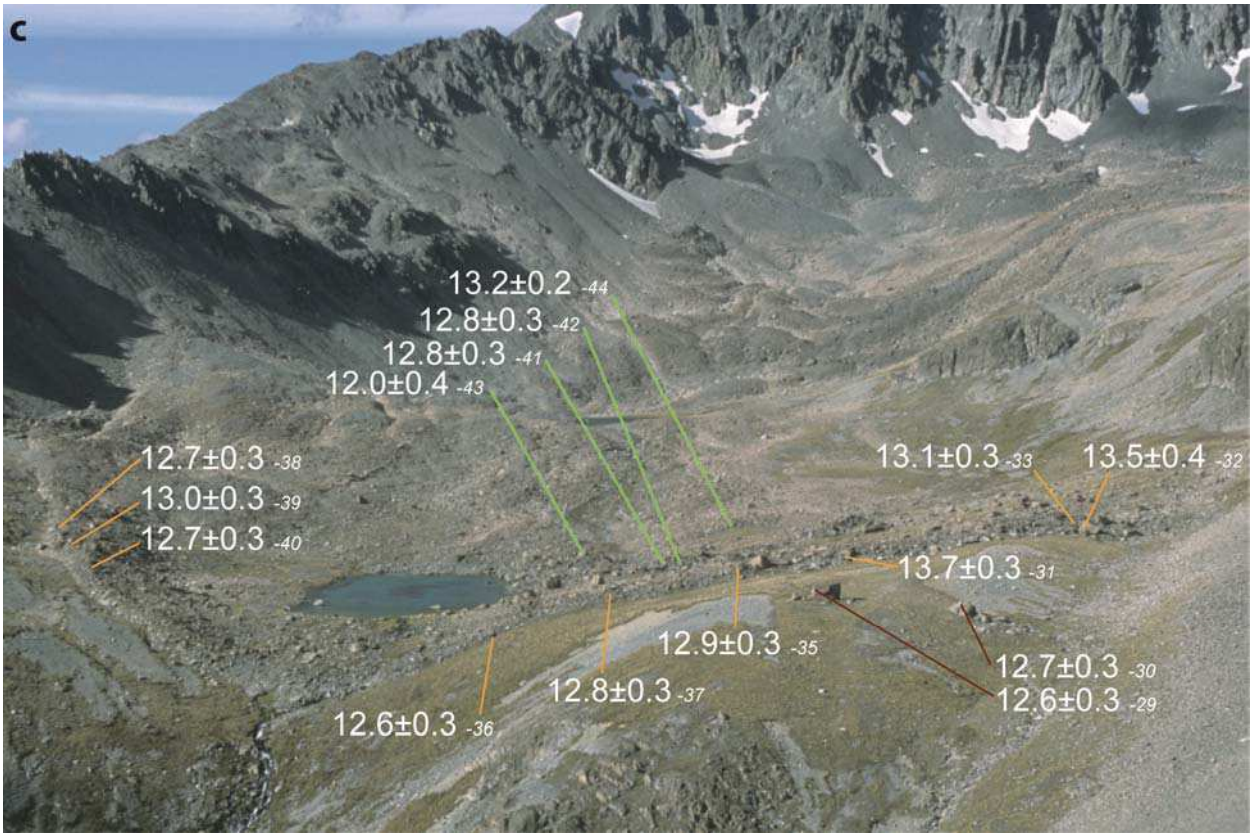

Figure S1 (continued). c, A photograph of Irishman basin that focuses in particular on the outer moraine belt and adjacent samples (photo: G. Denton). Vantage is north. The locations of the ^{10}Be dated samples are indicated (individual ages are shown with 1σ analytical error), with the last part of the *sample label* (Table S2). Color of lines matches location symbols on Figure 1. In the background are inner moraine belts A and B (Fig. 1).

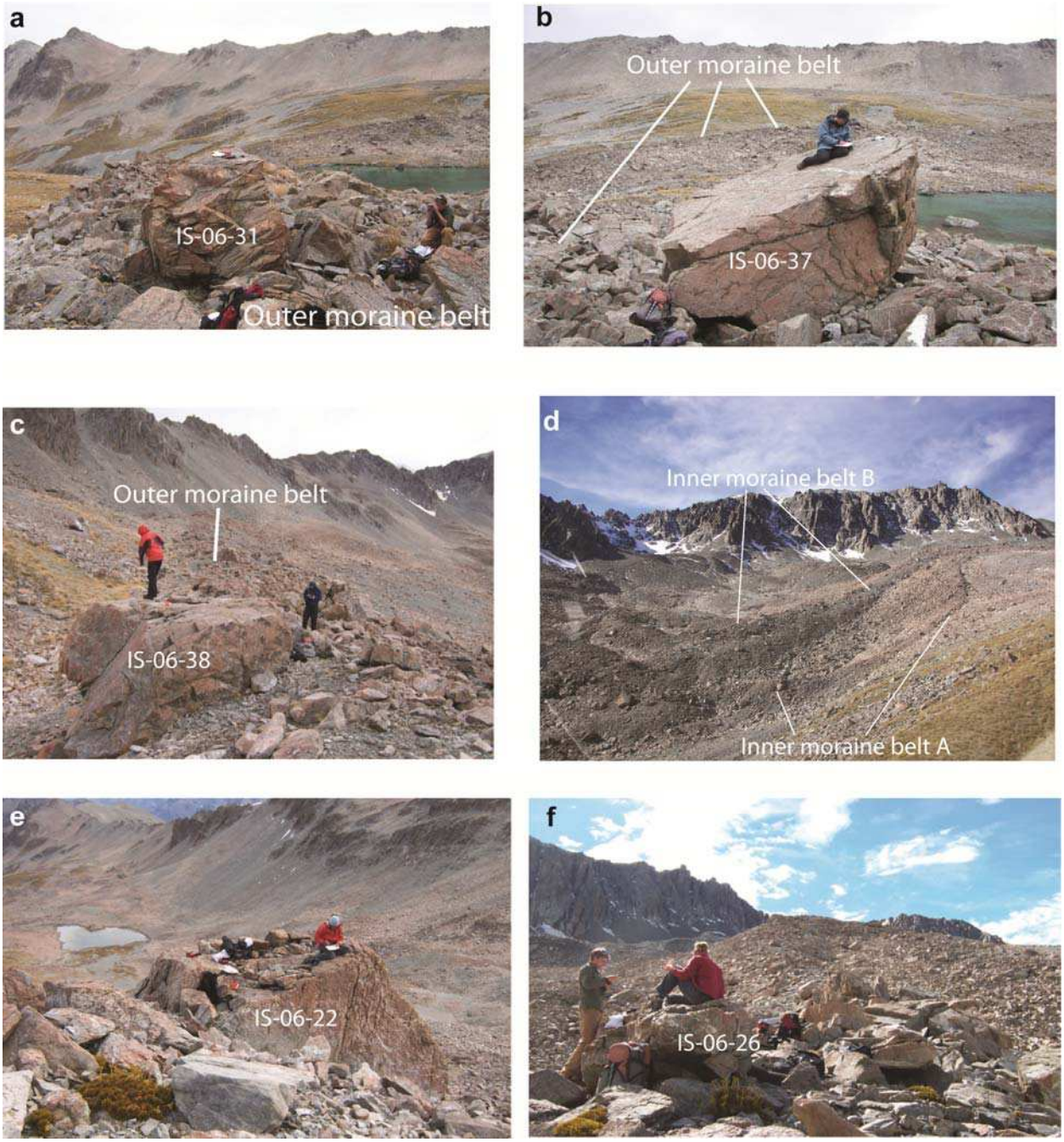

Figure S2. Photographs of boulder samples and moraines. a-c, Views of outer moraine belt and sampled boulders. Vantage is southwest and northwest (c). **d,** View of inner moraine belts A and B. The moraines are ~100 meters, or less, apart. Vantage is northeast. **e,** View of the basin from near sample IS-06-22. Vantage is southwest. **f,** View of inner moraine B (foreground to centre skyline) and inner moraine belt A (centre left). Vantage is northeast.

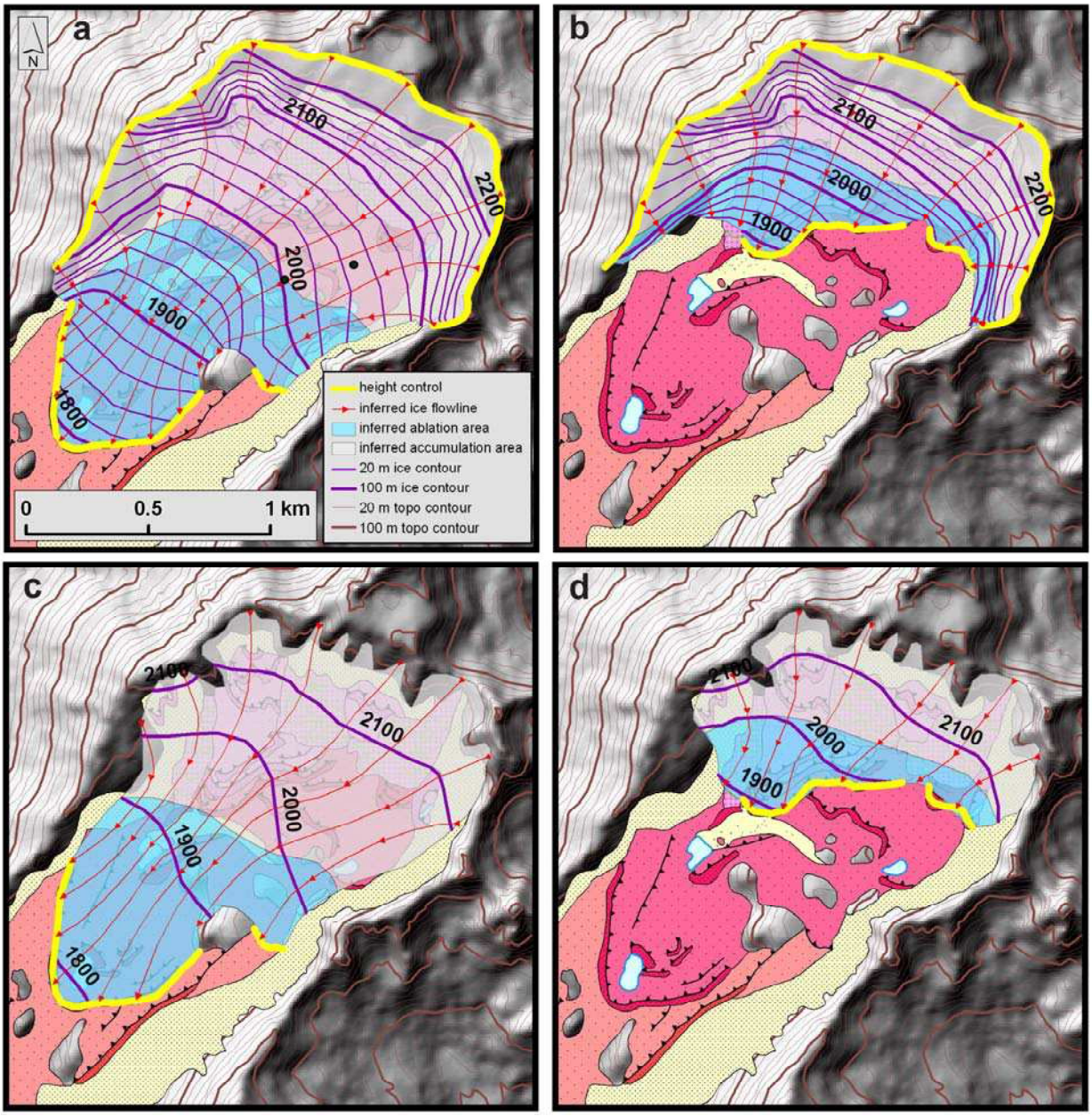

Figure S3. Reconstruction of the Irishman basin glacier and estimates of the ELA at ~13 and ~12 kyr ago, when the ice margin was at the outer moraine belt and inner moraine belt A, respectively (Table S3, see text). a-b, Larger ice volume model at ~13 and ~12 kyr ago, respectively. Two small black circles in Figure S3a are locations of striation measurements; **c-d,** Smaller ice volume model at ~13 and ~12 kyr ago, respectively.

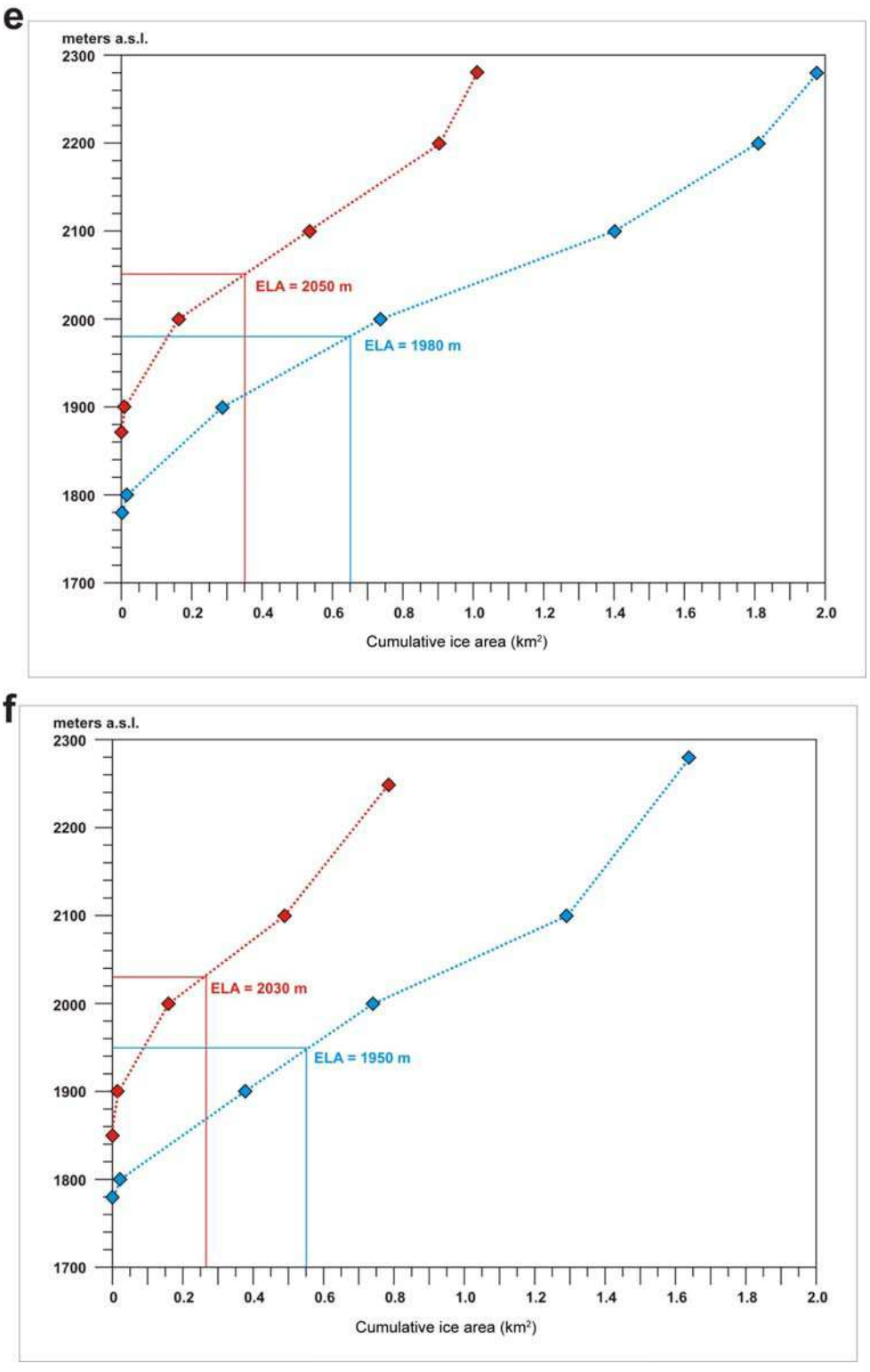

Figure S3 (continued). e, For larger ice volume model, cumulative area of glacier versus elevation (Fig. S3a, b) and ELA at ~13 and ~12 kyr ago; **f,** For smaller ice volume model, cumulative area of glacier versus elevation (Fig. S3c,d) and ELA at ~13 and ~12 kyr ago. We highlight that the ELA increase from the ~13 kyr outer moraine belt to the inner moraine A is similar (~70-80 m), whether the minimum or maximum reconstructions are used.

Figure S4. Probability distribution plots of boulder and moraine ages for Irishman basin. Individual ages are shown by thin black curves with 1σ uncertainties. The thick black line represents the probability distribution of the respective age population (normalized to 1). Arithmetic mean is indicated by the central vertical line, ±1σ range given by width of yellow rectangle, ±2σ range given by red lines, and ±3σ range given by outermost vertical lines. A production rate uncertainty of 2.2% is used based on the results in ref 13. In the text, the arithmetic mean ages are presented with an error that includes propagation of the analytical uncertainty and the uncertainty of the local production rate used (underlined value).

Distribution plots of ages are presented first for the outer moraine belt and second for inner moraine belt B, which are the outer and inner moraines dated and bracket the ~1500 yr period of ice recession in this study (Figs. S4a and S4b). The four samples on the intermediate moraines in the outer part of the basin (Fig. S4c) provide indistinguishable ^{10}Be ages (±1σ) from the adjacent outer moraine belt crest. In fact, inclusion of these four samples in the distribution for the outer moraine belt provides a mean age of 12.9±0.4 kyr for all thirteen samples, indistinguishable from 13.0±0.5 kyr (i.e., Fig. S4a). Nonetheless, based on geomorphic grounds (i.e., the samples are on different crests), we present them in a separate distribution. In the inner part of Irishman basin, ^{10}Be ages on boulders from the inner intermediate crests and inner moraine belt A are also statistically indistinguishable (Fig. S4d and e), ~ 12 kyr.

The arithmetic or weighted mean, median, and peak ages are statistically indistinguishable for each moraine set (each is calculated before rounding off to three significant figures, Table 2). Thus, the datasets resemble normal distributions and for the discussion of moraine ages the findings and conclusions of the study are the same if the mean or median ages are used. Reduced chi-squared (χ^2) values are also ~1, except for the outer intermediate moraines (Fig. S4c, $\chi^2 = 2.6$).

Three samples are dated from isolated inner moraines under the high northeast headwall (06-01, 06-02 and 06-03). These are not included in any of the probability distribution plots because rock glacier activity has obscured the morphologic relationship between these landforms and the inner moraine ridges farther west. The ages indicate that these small isolated moraines formed from ice flowing off the northeast headwall during Late-glacial, or early Holocene, time. Lastly, two samples (IS-06-29 and 30, Fig. S1) were collected beyond the outer moraine belt. These are not on moraine crests and their geomorphic context is unknown in relation to the outer moraine belt. Thus, they are not included in the above distribution.

a, The prominent **`outer moraine belt'** ridge that crosses the valley (Fig. S1). Samples include (n=9) IS-06-31, -32, -33, -35, -36, -37, -38, -39, and -40 and all boulders are from the same crest.

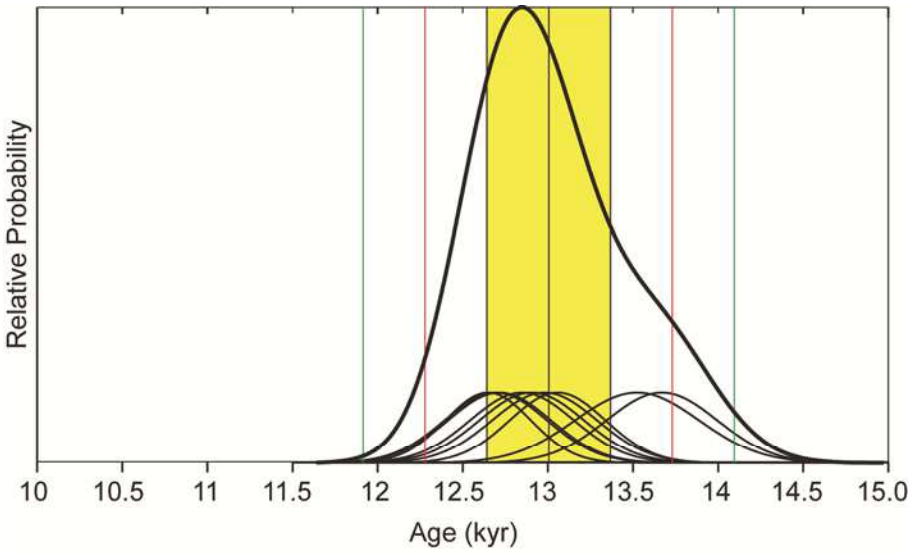

Statistics:
Arithmetic mean/1 sigma uncertainty: 13,000±360 yrs
Including production rate uncertainty: 13,000±460 yrs

Weighted mean/weighted uncertainty: 13,000±100 yrs
Peak age: 12,800 yrs
Median/Interquartile Range: 12,900±460 yrs
Reduced χ^2: 1.3

b, The **innermost** moraine crest dated, inner moraine belt B (Fig., 1). Samples include (n=5) IS-06-21, -22, -23, -26 and -27 and all ages are on boulders from the same crest.

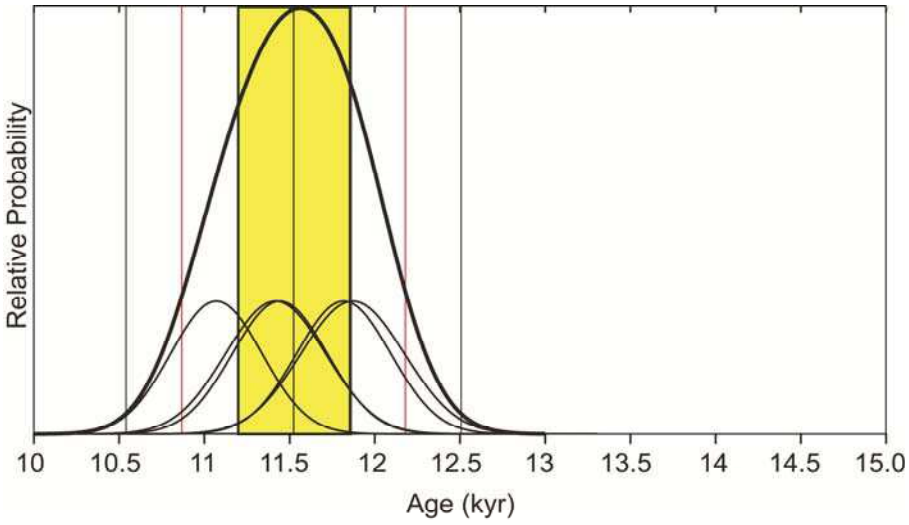

Statistics:
Arithmetic mean/1 sigma uncertainty: 11,500±330 yrs
Including production rate uncertainty: 11,500±420 yrs

Weighted mean/weighted uncertainty: 11,500±130 yrs
Peak age: 11,600 yrs
Median/Interquartile Range: 11,400±500 yrs
Reduced χ^2: 1.4

c, The **<u>intermediate</u>** moraines (Fig. 1) in the outer part of the Irishman basin that are close to the outer moraine belt. Samples include (n=4) IS-06-41, -42, -43, and -44.

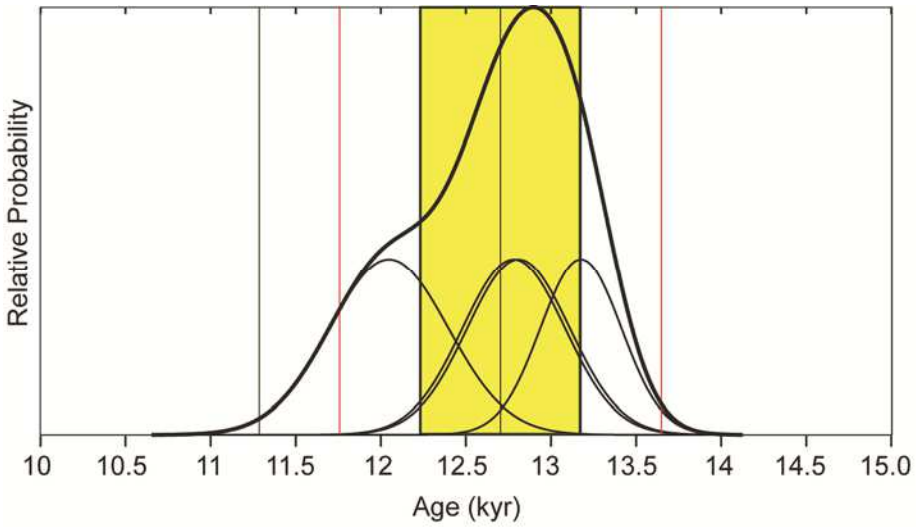

Note that IS-06-43 is more than 1σ different from the other three samples (but not at 2σ and thus it is included in the statistics), and hence the χ2 is slightly higher than for the distributions shown in Figures S4a-d.

<u>Statistics:</u>
Arithmetic mean/1 sigma uncertainty: 12,700±470 yrs
Including production rate uncertainty: <u>12,700±550 yrs</u>

Weighted mean/weighted uncertainty: 12,800±140 yrs
Peak age: 12,900 yrs
Median/Interquartile Range: 12,800±580 yrs
Reduced χ^2: 2.6

d, The **inner intermediate crests** (Fig. 1). Samples include (n=8) IS-06-15, -47, and -49.

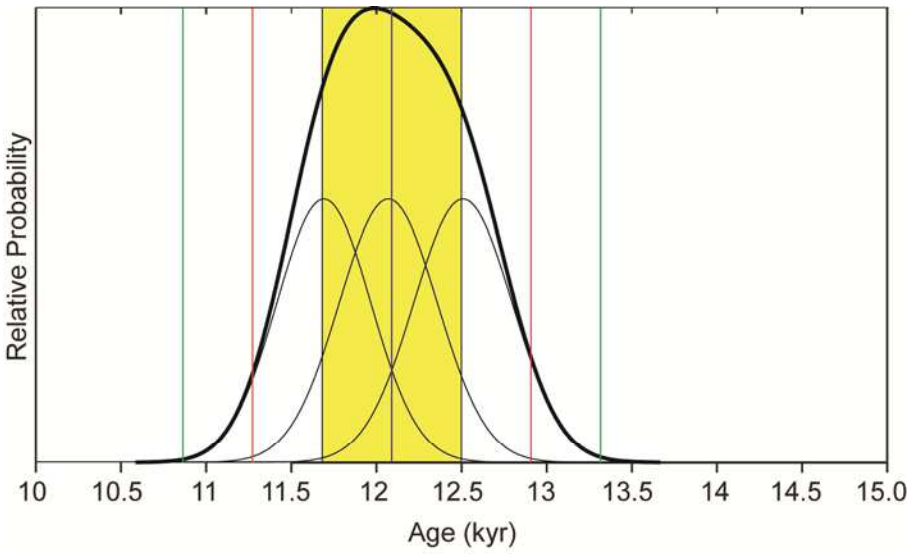

Statistics:
Arithmetic mean/1 sigma uncertainty: 12,100±410 yrs
Including production rate uncertainty: 12,100±490 yrs

Weighted mean/weighted uncertainty: 12,100±160 yrs
Peak age: 12,000 yrs
Median/Interquartile Range: 12,100±610 yrs
Reduced χ^2: 2.1

e, Inner moraine belt A (Fig. 1). Samples include (n=8) IS-06-18, -19, -24, -25, -28.

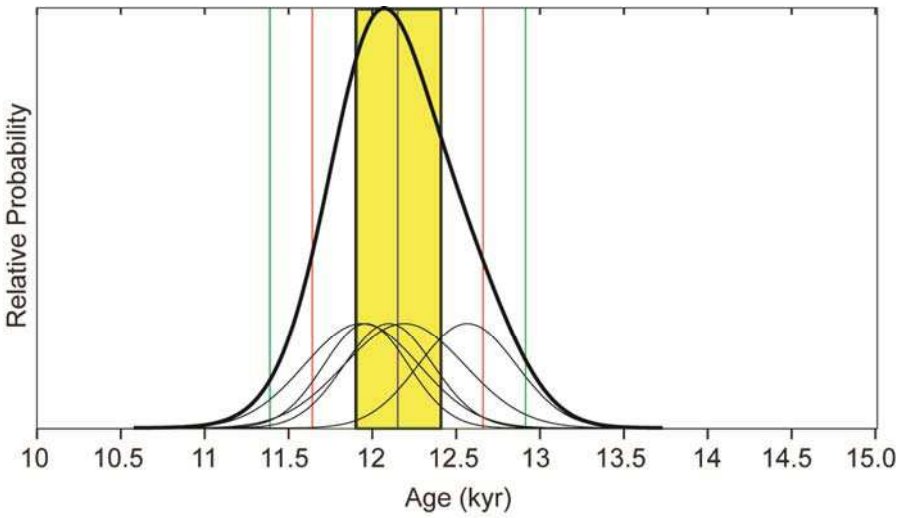

Note that IS-06-16, 17 and 20 are excluded from the plot as they are different at 3σ compared with the other ages on the same intermediate moraine crests. IS-06-16 was re-measured, which confirmed the anomalously young exposure age obtained at first measurement.

Statistics:
Arithmetic mean/1 sigma uncertainty: 12,200±250 yrs
Including production rate uncertainty: 12,200±370 yrs

Weighted mean/weighted uncertainty: 12,100±130 yrs
Peak age: 12,100 yrs
Median/Interquartile Range: 12,100±330 yrs
Reduced χ^2: 0.8